Monatsh Chem (2011) 142:233–242
DOI 10.1007/s00706-011-0454-1

ORIGINAL PAPER

Multi-walled carbon nanotubes as electrode materials for electrochemical studies of organometallic compounds in organic solvent media

Nikos G. Tsierkezos · Paweł Szroeder · Uwe Ritter

Received: 15 September 2010 / Accepted: 30 January 2011 / Published online: 24 February 2011

Abstract Films of vertically aligned multi-walled carbon nanotubes (MWCNT) were selectively synthesized on silicon dioxide substrate by catalytic chemical vapor deposition using either benzene or acetonitrile as carbon source and ferrocene (1% w/w) as catalyst. The MWCNT were extensively characterized by using scanning electron microscopy, transmission electron microscopy, thermogravimetric analysis, and Raman spectroscopy. In order to examine the prospective application of the fabricated MWCNT films for the detection of electro-active compounds in organic solvent media, electrochemical studies of the oxidation of cobaltocene ($CoCp_2$) to cobaltocenium cation ($CoCp_2^+$) (Cp = cyclopentadienyl anion) in acetonitrile were performed on these films. For this purpose, cyclic voltammetry and electrochemical impedance spectroscopy were employed. The electrochemical parameters for the $CoCp_2^{+/0}$ couple in acetonitrile were derived and compared with those obtained using a conventional glassy carbon electrode. The results demonstrate that the synthesized MWCNT films are promising electrode materials for the electrochemical detection of electro-active species in organic solvents. The MWCNT film formed upon decay of benzene has higher capacitance, less Warburg impedance, and less charge transfer resistance, and consequently it provides faster electron transfer kinetics.

N. G. Tsierkezos (✉) · U. Ritter
Institut für Chemie, Elektrochemie und Galvanotechnik, Fachgebiet Chemie, Technische Universität Ilmenau, Weimarer Str. 25, 98693 Ilmenau, Germany
e-mail: nikos.tsierkezos@tu-ilmenau.de

P. Szroeder
Instytut Fizyki, Uniwersytet Mikołaja Kopernika, Grudziadzka 5/7, 87-100 Toruń, Poland

Keywords Cobaltocene · Cyclic voltammetry · Electrochemical impedance spectroscopy · Multi-walled carbon nanotubes · Raman spectroscopy

Introduction

Carbon exhibits a richness of allotropes with different types of carbon–carbon bonds and consequently dissimilar physical and chemical properties. The recently discovered new forms of carbon, such as fullerenes and carbon nanotubes, have already attracted the interest of many scientists because they have promising potential applications in the field of nanoscience [1–3]. Because of their unique structure and their physical, mechanic, chemical, and electronic properties, carbon nanotubes (CNTs) are potentially useful in many applications such as nanotechnology, electronics, optics, and other fields of material science, as well as in architecture and biomedical fields. CNTs are probably the strongest substances that will ever exist with a tensile strength greater than steel but only one sixth of its weight. A detailed literature search revealed that in the recent years many researchers have been involved in extensive theoretical and experimental investigation of CNTs. It is remarkable that in a very short duration CNTs have drawn the attention of both industry and academia [4, 5]. CNTs are allotropes of carbon having a cylindrical nanostructure, which can be conceptualized by wrapping a thick graphite layer into a cylinder, with a length-to-diameter ratio typically ranging from 100:1 to 10,000:1. However, it is important to mention that CNTs with a length-to-diameter ratio up to 28,000,000:1, the largest amongst all known materials, were recently constructed [6]. CNTs exhibit unique physical and electrical properties, such as high electric conductivity, thermal and chemical stability, as well as remarkable mechanical

strength. The unique strength of CNTs is attributed to their chemical bonding, which is composed entirely of bonds between sp^2-hybridized carbon atoms similar to those of graphite. The properties of CNTs depend on their structure. Consequently, methods for their synthesis aim to produce CNTs with controlled diameter, length, chirality, and the number of graphite walls [7]. CNTs are assigned into two classes: single-walled (SWCNT) and multi-walled carbon nanotubes (MWCNT). The former consist of a single graphite sheet rolled flawlessly to produce a tube, whereas the latter comprise several concentric tubes fitted one inside the other [8]. Catalytic chemical vapor deposition (CVD) is an efficient and selective for the synthesis of either SWCNT or MWCNT [9, 10]. The formation of CNTs via the CVD method takes place through the decomposition of carbon-containing compounds on the surface of nanometer-sized transition metal particles, such as iron, cobalt, or nickel, that act as catalyst for the decomposition of the carbon source and concomitantly serve as the CNT formation sites, on which the CNTs nucleate and grow. Organometallic compounds of iron such as ferrocene or iron pentacarbonyl were successfully used as catalysts for CNT synthesis by CVD [11].

Recently CNTs gained considerable attention as perfect substrates in the field of the electrochemistry either for studying elemental processes of electron transfer, or for electroanalytical applications [12, 13]. Taking into consideration that CNTs have the ability to carry large current densities and provide fast electron transfer kinetics [14], the area of electrochemistry seems to be one of the most productive in terms of applications, especially in the field of sensors or biosensors and nanoelectrodes. A literature search revealed that many researchers applied CNT electrodes in electroanalysis for detection of molecules with biological interest. For example, Deo and Wang [15] used glassy carbon electrodes modified with CNT coatings for the catalytic oxidation of galactose, whereas Musameh et al. [16] applied a CNT-modified glassy carbon electrode for the detection of β-nicotinamide adenine dinucleotide (NADH). Furthermore, CNT electrodes were successfully applied as working electrodes for electrochemical studies of uric acid and L-ascorbic acid [17], cytochrome *C* [18], and morphine [19]. It is important, however, to note that the production of electrodes from SWCNT is complicated and therefore the development and application of such electrodes in electroanalysis appears to be limited, on the basis of reported literature, compared to the production and application of MWCNT electrodes, which show promising electrochemical properties [20].

The present article reports the electrochemical investigation of the oxidation of $CoCp_2$ to $CoCp_2^+$ on fabricated MWCNT films by means of cyclic voltammetry (CV) and electrochemical impedance spectroscopy (EIS). The extracted results are compared with those obtained using a conventional glassy carbon (GC) electrode. The MWCNT films used in the present work were synthesized by catalytic CVD upon decomposition of either benzene (BZ) or acetonitrile (ACN) using ferrocene (1% w/w) as catalyst. $CoCp_2^{+/0}$ was selected as the reference redox couple for the present investigation because the mechanism and the electrochemical parameters of this model system were investigated and reported previously [21]. In the present work two kinds of MWCNT films will be presented: the $MWCNT_{BZ}$ film, produced upon decomposition of BZ; and the $MWCNT_{ACN}$ film, produced upon decay of ACN. The synthesized MWCNT films were extensively characterized by using SEM, transmission electron microscopy (TEM), thermogravimetric analysis (TGA), and Raman spectroscopy.

Results and discussion

TEM/SEM

Figure 1 shows representative TEM images of the synthesized $MWCNT_{BZ}$ film. The diameter of the inner tube varies from 5 to 10 nm, whereas the diameter of the outer tube varies from 20 to 50 nm. Figure 2 shows typical SEM images of the synthesized MWCNT films upon decay of either BZ or ACN. The low magnification SEM images show the uniformity of the film area and the CNT length, and the high magnification the CNT diameter. It can be seen that by varying the carbon source the arrangement of the formed MWCNT is modified. The SEM images reveal that when ACN is used as carbon precursor the "packing organization" of the aligned MWCNT on the film is rather enhanced (Fig. 2a), whereas the MWCNT arrangement becomes quite worse when BZ is used as carbon source material (Fig. 2b). This high degree of roughness of the surface of the $MWCNT_{BZ}$ film is expected to improve its real active surface area. Thus, for $MWCNT_{BZ}$ and $MWCNT_{ACN}$ films with the same geometrical area, the former seem to have twice the real active surface area of the latter. Furthermore, the conductivity data show higher current response on the $MWCNT_{BZ}$ electrode compared to $MWCNT_{ACN}$. In other words the results indicate more conductive areas in $MWCNT_{BZ}$ (5.64×10^{-3} S) than in $MWCNT_{ACN}$ (3.56×10^{-3} S). Anyhow, the current response on both MWCNT films seems to be significantly larger compared to that on the "bare" SiO_2 film (0.11×10^{-6} S).

Raman spectroscopy

Figure 3 shows the Raman spectra of MWCNT grown upon decomposition of either BZ or ACN. The Raman features associated with the carbon nanotube tangential

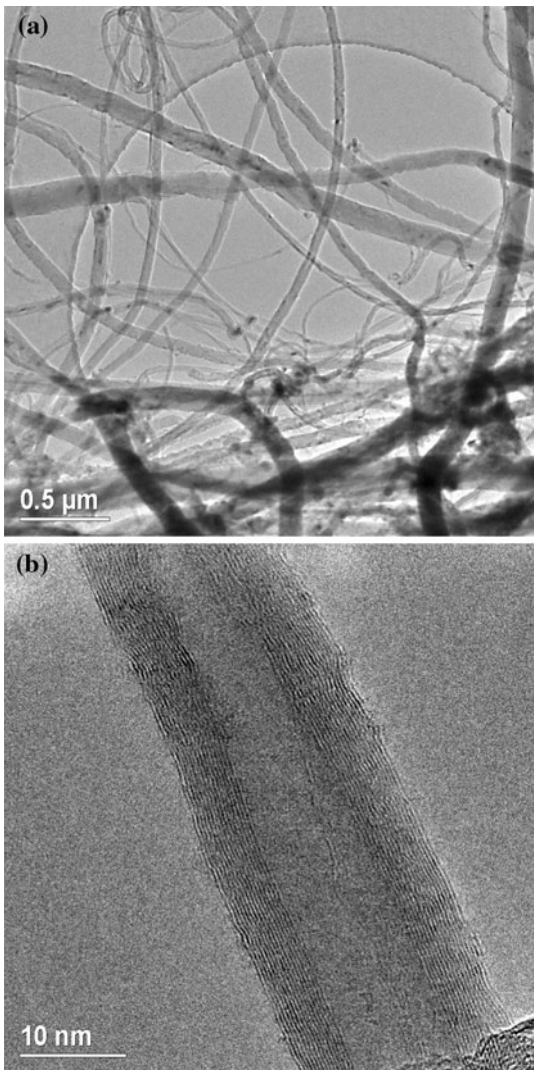

Fig. 1 TEM micrographs of $MWCNT_{BZ}$

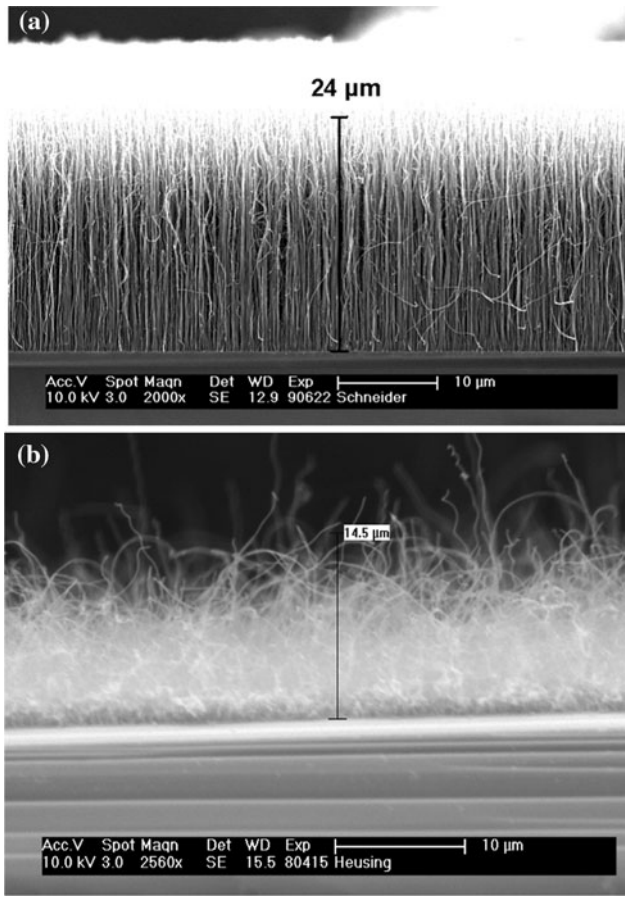

Fig. 2 Typical SEM images of $MWCNT_{ACN}$ (**a**) and $MWCNT_{BZ}$ (**b**) films synthesized on SiO_2 substrate by CVD using $FeCp_2$ as catalyst (1% w/w) and ACN and BZ as carbon sources. The SEM images were obtained with an accelerating voltage of 10 kV and magnification factors of either ×2,000 (**a**) or ×2,560 (**b**). The measured average thickness of the synthesized $MWCNT_{ACN}$ and $MWCNT_{BZ}$ films was 24 and 15 μm, respectively

mode at about 1,590 cm^{-1} (G band) together with the disorder-induced mode at about 1,289 cm^{-1} were observed. The G mode involves the in-plane bond-stretching oscillations of sp^2 carbon atom pairs. Its position in the recorded spectra is shifted to higher frequencies (about 10 cm^{-1}) from that of perfect graphite. In the case of $MWCNT_{ACN}$ the G band is split into the G^- (at 1,582 cm^{-1}) and the G^+ mode (at 1,592 cm^{-1}). Such effects can be explained by phonon confinement in small diameter tubes [22]. In the case of $MWCNT_{BZ}$ the double-peak G band splitting disappeared. This is probably due to disorder and larger diameters of the graphene tubes. In this case the G feature exhibits a weakly asymmetric line-shape with a peak appearing at 1,592 cm^{-1}. The spectra recorded for $MWCNT_{BZ}$ have additional features in the range 1,600–1,900 cm^{-1} which are not observed in $MWCNT_{ACN}$. A line at 1,758 cm^{-1} can be assigned to the stretching oscillations of C=O bonds of carbonyl groups.

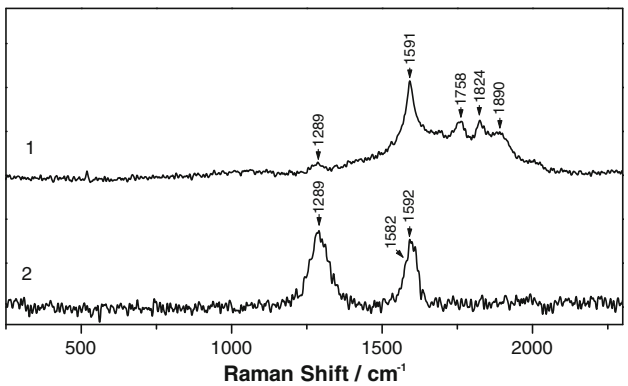

Fig. 3 Raman spectra of $MWCNT_{BZ}$ (*1*) and $MWCNT_{ACN}$ (*2*)

The shoulders at 1,824 cm^{-1} and 1,890 cm^{-1} are typical of defective graphene materials [23]. The D mode is forbidden in perfect graphite and only occurs in the presence of

disorder. Its intensity is strictly connected to the presence of sixfold aromatic rings and in contrast to perfect graphite it indicates the degree of ordering in the investigated systems [24]. In the case of $MWCNT_{ACN}$ the intensity of the D mode appears to be much higher compared to that of $MWCNT_{BZ}$, and this finding indicates that $MWCNT_{ACN}$ consists of tubes containing larger aromatic ring areas. This observation is in agreement with the obtained SEM images (Fig. 1), in which the structure and degree of ordering of $MWCNT_{ACN}$ appear to be enhanced.

Cyclic voltammetry

CV and EIS were used to investigate the electrochemical response and consequently the quality of the fabricated MWCNT films in organic solvent media. For this purpose $CoCp_2^{+/0}$ was used as the reference redox couple for all electrochemical measurements. Representative cyclic voltammograms recorded for the oxidation of $CoCp_2$ to $CoCp_2^+$ on $MWCNT_{BZ}$ and $MWCNT_{ACN}$ working electrodes at various scan rates (v) are shown in Figs. 4 and 5, respectively. For comparison, the cyclic voltammograms recorded on $MWCNT_{BZ}$, $MWCNT_{ACN}$, and GC working electrodes at $v = 0.10$ V s^{-1} are shown in Fig. 6. The electrochemical results obtained for all investigated electrodes at $v = 0.10$ V s^{-1} are summarized in Table 1. As can be seen in Fig. 4, the cyclic voltammograms recorded on $MWCNT_{BZ}$ are symmetric with equal cathodic (E_p^{red}) and anodic (E_p^{ox}) peak currents, and consequently the ratio i_p^{ox}/i_p^{red} is equal to unity. Similar behavior was observed for the GC electrode (Fig. 6). The corresponding cyclic voltammograms recorded on $MWCNT_{ACN}$ (Fig. 5) seem to be

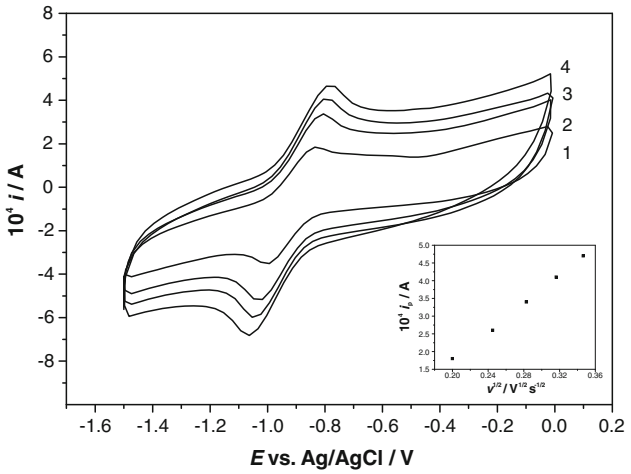

Fig. 4 Cyclic voltammograms recorded for $CoCp_2$ (1.0×10^{-3} mol dm^{-3}) in ACN (0.1 mol dm^{-3} $TBAPF_6$) on a $MWCNT_{BZ}$ electrode at $v = 0.04$ V s^{-1} (*1*), $v = 0.08$ V s^{-1} (*2*), $v = 0.10$ V s^{-1} (*3*), and $v = 0.12$ V s^{-1} (*4*). *Inset* variation of oxidative peak current (i_p^{ox}) with the square root of scan rate ($v^{1/2}$)

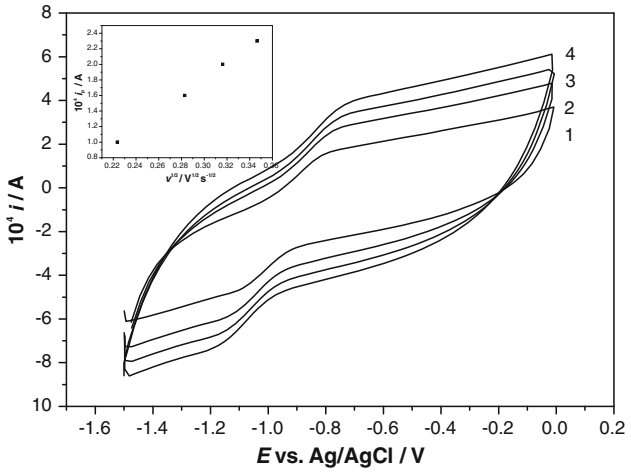

Fig. 5 Cyclic voltammograms recorded for $CoCp_2$ (1.0×10^{-3} mol dm^{-3}) in ACN (0.1 mol dm^{-3} $TBAPF_6$) on a $MWCNT_{ACN}$ electrode at $v = 0.05$ V s^{-1} (*1*), $v = 0.08$ V s^{-1} (*2*), $v = 0.10$ V s^{-1} (*3*), and $v = 0.12$ V s^{-1} (*4*). *Inset* variation of oxidative peak current (i_p^{ox}) with the square root of scan rate ($v^{1/2}$)

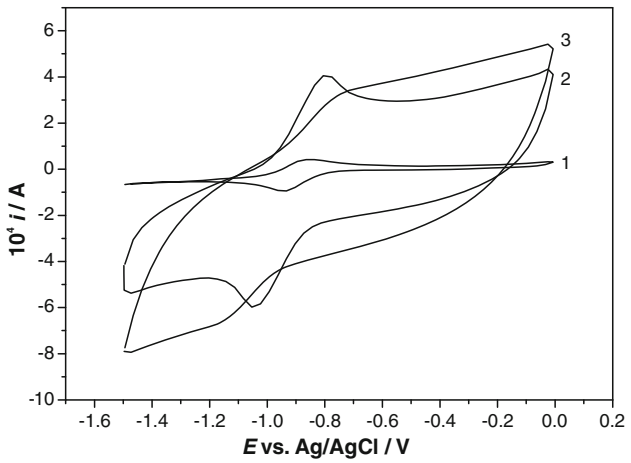

Fig. 6 Cyclic voltammograms recorded for $CoCp_2$ (1.0×10^{-3} mol dm^{-3}) in ACN (0.1 mol dm^{-3} $TBAPF_6$) on GC (*1*), $MWCNT_{BZ}$ (*2*), and $MWCNT_{ACN}$ (*3*) electrodes at $v = 0.10$ V s^{-1}

somehow "disturbed", compared to those obtained on either GC or $MWCNT_{BZ}$ electrodes, but in any case the ratio i_p^{ox}/i_p^{red} also approaches unity ($i_p^{ox}/i_p^{red} \approx 1.1$). Note that by repeating the experiments with three other MWCNT films also synthesized upon decomposition of ACN, the same behavior was observed, namely similarly "disturbed" cyclic voltammograms were obtained. As can be seen in Fig. 6, the peak current obtained on $MWCNT_{BZ}$ film seems to be somehow larger compared to the peak current obtained on $MWCNT_{ACN}$. Furthermore, it is obvious that both MWCNT films have rather larger peak current compared to that obtained on the GC electrode. Indeed, the peak current obtained on $MWCNT_{BZ}$ appears to be twice that obtained on $MWCNT_{ACN}$ and about eight times that obtained on GC. In detail, the anodic peak

Table 1 Electrochemical results obtained for the oxidation $CoCp_2$ (1.0×10^{-3} mol dm^{-3}) in ACN (0.1 mol dm^{-3} $TBAPF_6$) on GC, $MWCNT_{BZ}$, and $MWCNT_{ACN}$ films at the scan rate of $v = 0.10$ V s^{-1}

Electrodes	GC	$MWCNT^{gi}_{BZ}$	$MWCNT^{hi}_{ACN}$
E_p^{ox} (V)[a]	−0.862	−0.802	−0.765
E_p^{red} (V)[a]	−0.936	−1.036	−1.091
$E_{1/2}$ (V)[a]	−0.899	−0.919	−0.928
ΔE (V)	0.074	0.234	0.326
10^4 i_p^{ox} (A)	0.41	3.10	1.50
i_p^{ox}/i_p^{red}	1.00	1.00	1.13
a[b]	0.50	0.50	0.50
10^3 k_s (cm s^{-1})	25.35[c]/25.20[j]	1.50[c]/1.68[j]	0.66[c]/0.88[j]
10^4 I_o (A)[d]	11.1	5.9	1.5
R_s (Ω)[e]	26.7	108.7	114.0
R_{ct} (Ω)[e]	22.8	42.9	170.0
10^6 C_{dl} (F)[e]	11.62	2.42	1.20
σ (kΩ s$^{-1/2}$)	34.06	0.32	0.25
% Error[f]	0.7	0.8	0.9

E_p^{ox} and E_p^{red}, anodic and cathodic peak potential, respectively; $E_{1/2}$, half-wave potential; ΔE_p, peak potential separation; i_p^{ox}, anodic peak current; i_p^{ox}/i_p^{red}, anodic and cathodic peak current ratio; a, transfer coefficient; k_s, heterogeneous electron transfer rate constant; I_o, exchange current; R_s, electrolyte resistance; R_{ct}, charge transfer resistance; C_{dl}, double layer capacitance; σ, Warburg parameter

[a] All potentials are reported vs. Ag/AgCl (KCl sat.)

[b] The a values were determined from the relation: $a = (E_p^{ox} - E_{1/2})/(E_p^{ox} - E_p^{red})$ [52]

[c] The k_s values were determined from Nicholson relation, Eqs. 1 and 2

[d] The I_o values were determined from Eq. 3

[e] The EIS parameters were determined by simulation using the software Thales (version 4.15)

[f] Corresponding % maximum mean impedance errors which arise from the simulation of the EIS spectra

[g] The MWCNT film was produced upon decomposition of BZ

[h] The MWCNT film was produced upon decomposition of ACN

[i] The real active surface areas of the $MWCNT_{BZ}$ and $MWCNT_{ACN}$ films were determined as 0.64 and 0.31 cm^2, respectively

[j] The k_s values were determined from EIS data according to Eq. 6

current at $v = 0.10$ V s^{-1} decreases in the following order: $MWCNT_{BZ}$ ($i_p^{ox} = 310$ μA) > $MWCNT_{ACN}$ ($i_p^{ox} = 150$ μA) > GC ($i_p^{ox} = 41$ μA). This behavior can be explained most probably by the decrease of the real active surface area of the electrodes, which occurs in the same order: $MWCNT_{BZ}$ (0.64 cm^2) > $MWCNT_{ACN}$ (0.31 cm^2) > GC (0.08 cm^2). Note that in all cases a linear variation of the peak current with the square root of the scan rate was observed (inset Figs. 4, 5).

The half-wave potential ($E_{1/2}$) values of the couple $CoCp_2^{+/0}$ determined as the average value of E_p^{ox} and E_p^{red} [25] were found to be slightly dependent on the working electrode material. It has been observed that by replacing the GC with MWCNT films the $E_{1/2}$ of $CoCp_2^{+/0}$ is shifted by about 25 mV in the negative direction. Considering that the experimental potential uncertainty is no more than ±5 mV, the shifting of $E_{1/2}$ in the negative direction indicates that the oxidation of $CoCp_2$ to $CoCp_2^+$ takes place easily on MWCNT films compared to the GC electrode. It would be very useful to compare the $E_{1/2}$ values for $CoCp_2^{+/0}$ determined on MWCNT films with published $E_{1/2}$ values measured in either ACN or other organic solvents. Thus, the $E_{1/2}$ value of −0.92 V vs. Ag/AgCl obtained on MWCNT films after normalization with respect to the $FeCp_2^{+/0}$ couple is converted to the $E_{1/2}$ value of −1.34 V vs. $FeCp_2^{+/0}$ (considering that $E_{1/2}$ of $FeCp_2^{+/0}$ is 0.42 V vs. Ag/AgCl) which is slightly more negative that the $E_{1/2}$ values of −1.33 V vs. $FeCp_2^{+/0}$ and −1.31 V vs. $FeCp_2^{+/0}$ obtained for $CoCp_2^{+/0}$ in methylene chloride and glyme, respectively [26]. Furthermore, the literature values of $E_{1/2} = -1.34$ V vs. $FeCp_2^{+/0}$ [27], $E_{1/2} = -1.35 \pm 0.01$ V vs. $FeCp_2^{+/0}$ [28], and $E_{1/2} = -1.345$ V vs. $FeCp_2^{+/0}$ [29] for $CoCp_2^{+/0}$ in ACN are in absolute agreement with the value of $E_{1/2} = -1.34$ V vs. $FeCp_2^{+/0}$ measured on MWCNT in the present work.

The anodic and cathodic peak potential separation (ΔE_p) obtained on MWCNT films was found to be strongly dependent on the potential scan rate (v), namely the variation of ΔE_p on v was found to be almost linear. As an example, a representative curve of the variation of ΔE_p with v for the $MWCNT_{BZ}$ film is shown in Fig. 7. In detail, the determined ΔE_p values for the $MWCNT_{BZ}$ film in the investigated scan rate range (0.04–0.12 V s^{-1}) were between 0.143 and 0.264 V, whereas for the $MWCNT_{ACN}$ film obviously quite larger ΔE_p values were obtained (0.255–0.386 V). The findings indicate high electrode

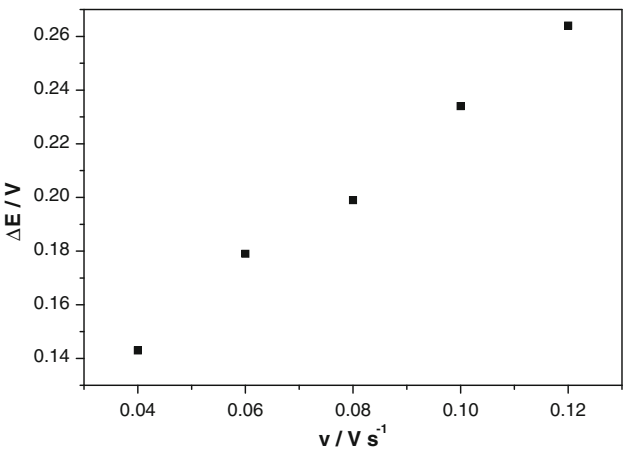

Fig. 7 Anodic and cathodic peak potential separation (ΔE_p) vs. the potential scan rate (v) obtained for $CoCp_2$ (1.0×10^{-3} mol dm^{-3}) in ACN (0.1 mol dm^{-3} $TBAPF_6$) on $MWCNT_{BZ}$ film

resistance and a quasi-reversible process on MWCNT films. In contrast, the ΔE_p value obtained on the GC electrode ($\Delta E_p = 0.070$ V) was found to be slightly dependent on the scan rate and very close to the ideal value that is indicative of a reversible one-electron transfer and diffusion-controlled process ($\Delta E_p = 0.060$ V at 298.15 K) [30]. Because the peak separation gives an estimation of the kinetics of the electron transfer process, and thus it can be used for the determination of the heterogeneous electron transfer rate constant (k_s) (see next paragraph), one can initially consider that the smaller the peak separation the higher the electron transfer constant rate. Consequently, the larger ΔE_p values obtained on MWCNT films indicate that the electron transfer process occurring on these electrodes is slower compared to that on the GC electrode. However it is possible that the large ΔE_p values obtained for the MWCNT films can be also attributed to some extent on uncompensated resistance effects, which seem to be rather significant in solutions of organic solvent media because of their low polarity (low dielectric constant). Anyhow, considering that the total amount of resistance which was not compensated is approximately the same for both MWCNT films, the obtained difference in ΔE_p values and therefore the difference of the determined k_s values for the MWCNT films reflect their dissimilar rates for the electron transfer process. In order to determine the k_s values of the investigated $CoCp_2^{+/0}$ redox couple on either MWCNT or GC electrodes the procedure described by Nicholson [31] was applied. Briefly, this process relates k_s to ΔE_p through a working curve of the dimensionless kinetic parameter ψ. According to Nicholson [31], large ψ values characterize a reversible electron transfer process, intermediate ψ values characterize a quasi-reversible process, whereas when $\psi \approx 0$ the electron process can be recognized as totally irreversible. For the present work the values of ψ were calculated from the experimental ΔE_p values according to the reference curve $\Delta E_p = f(\psi)$ which was plotted from the data reported in the literature [31]. The obtained ψ values and their corresponding sweep rates (v) can be used for the calculation of the k_s parameter from the following relations:

$$\psi = \frac{\gamma^a k_s}{\sqrt{n\pi F v D_o / RT}} \quad (1)$$

$$\gamma = \left(\frac{D_o}{D_R}\right)^{1/2} \quad (2)$$

where a is the charge transfer coefficient ($a = 0.5$); D_o and D_R are the diffusion coefficients of the oxidized and reduced species, respectively; n is the number of electrons involved in the reaction ($n = 1$); R is the gas constant; F is the Faraday constant; T is the temperature, and v is the scan rate. Actually, to apply the above relations the parameter γ must be known. However, except for the unusual case of a very large difference between D_o and D_R, the parameter γ for most of the redox couples is always very near unity. Consequently, considering that $D_o \approx D_R$ ($D_o = 3.25 \times 10^{-5}$ cm^2 s^{-1}) [21] the k_s values of the reference $CoCp_2^{+/0}$ couple on the investigated MWCNT and GC electrodes were determined and included in Table 1. The determined k_s values suggest that the electron transfer process occurring on the GC electrode is extremely faster ($k_s \approx 25 \times 10^{-3}$ cm s^{-1}) compared to the electron transfer process taking place on either $MWCNT_{BZ}$ ($k_s \approx 2 \times 10^{-3}$ cm s^{-1}) or $MWCNT_{ACN}$ ($k_s \approx 1 \times 10^{-3}$ cm s^{-1}) films, which is obviously rather slow. It is, however, very interesting that among the investigated MWCNT films a greater k_s value was obtained for the $MWCNT_{BZ}$ film, which was produced by using BZ as the carbon source (namely the k_s value obtained on $MWCNT_{BZ}$ appears to be twice that determined on $MWCNT_{ACN}$). This result can be partly attributed to the different arrangement and consequently the different degree of "disorder" of the aligned MWCNT on the surface of the synthesized MWCNT films, as was confirmed from the obtained SEM images (Fig. 2). Most probably the "packing organization" of the aligned MWCNT affects the electrochemical behavior of the constructed films, because it plays a main role in the interactions between the electroactive compound and the surface of the electrode. It is obvious that on the $MWCNT_{BZ}$ film, having a "harder" surface compared to the surface of the $MWCNT_{ACN}$ film, the interactions between $CoCp_2$ and electrode are amplified and thus the rate of the electron transfer reaction is increased. The conductivity of the synthesized MWCNT films is expected to affect significantly the rate of the electrochemical process. Thus, the $MWCNT_{BZ}$ film being more conductive than the $MWCNT_{ACN}$ film leads to higher k_s.

It would be very interesting to compare the results extracted in the present work with published electrochemical data obtained on CNT films for other compounds in ACN. Using a SWCNT-SiO_2 film, Yu et al. [32] obtained a peak potential separation of $\Delta E_p = 0.122$ V ($k_s = 5.89 \times 10^{-3}$ cm s^{-1}) for $FeCp_2$ dissolved in 0.1 mol dm^{-3} TBAP/ACN solution at a scan rate of 0.10 V s^{-1}, whereas Noel et al. [33] reported a ΔE_p value of 0.160 V ($k_s = 3.10 \times 10^{-3}$ cm s^{-1}) for the same system under the same conditions. The ΔE_p value of 0.143 V found in the present work on $MWCNT_{BZ}$ for $CoCp_2$ in ACN at $v = 0.040$ V s^{-1} seems to be within the same range of the literature ones.

Electrochemical impedance spectroscopy

Complementary information concerning the sensitivity and thus the quality of the synthesized MWCNT films can be obtained from EIS measurements. Such experiments give useful information regarding the mechanisms and suggest an equivalent electrical circuit that represents the investigated system. The EIS spectra, namely the Nyquist plots, recorded on the investigated $MWCNT_{BZ}$, $MWCNT_{ACN}$, and GC electrodes are shown in Fig. 8. In the Nyquist plots the complex impedance is presented as a sum of the real (Z_{re}) and imaginary (Z_{im}) components that originate mainly from the resistance and capacitance of the cell, respectively. As can be seen in Fig. 8, there are some significant differences in the recorded EIS spectra of the investigated electrodes. The EIS spectrum for the GC electrode reveals a linear impedance locus, namely a Warburg impedance response, with an angle of about 45° to the Z_{re}-axis. The early increase of the imaginary part of impedance and the absence of any indication of a semicircle at high frequencies indicate that the interfacial charge transfer process is very fast on this electrode [34]. This response suggests a reversible diffusion-controlled electron transfer process on this electrode and therefore the EIS spectrum supports the findings from the CV studies [35, 36]. In other words, this behavior indicates that the diffusion of the electro-active species in the solution prevails in the whole frequency region [37]. In contrast, the Nyquist plots obtained for $MWCNT_{BZ}$ and $MWCNT_{ACN}$ films show the appearance of a very well defined semicircle terminating in a line. In detail, the EIS spectra include a semicircle portion observed at higher frequencies that corresponds to the electron-transfer-limited process. This feature is followed by a linear part appearing at the lower frequency region that can be attributed to a diffusion-limited electron transfer [38]. Namely, the straight line reveals that the diffusion of the electro-active species prevails over the electron transfer in this frequency range. The respective semicircle diameter, obtained by extrapolation of the semicircle on the Z_{re}-axis, corresponds to the electron transfer resistance (R_{ct}) at the electrode surface, a parameter which is attributed to the electrochemical reaction and provides an estimation not only of the response of the electron transfer but also of the sensitivity of the electrode [39]. According to theory the development of such semicircles implies there is a barrier to the interfacial electron transfer (the system is under kinetic control) and it can be attributed to an increase of the passivity of the surface of the electrode through the formation of a coating. The presence of a coating on the electrode surface is expected to slow down the interfacial charge transfer kinetics which is reflected by an increase of R_{ct}. Furthermore, the appearance of a semicircle can be also attributed to partial degradation of the MWCNT film [40]. From a first view of the EIS spectra in Fig. 8 it can be recognized that the impedance semicircle and consequently the R_{ct} corresponding to $MWCNT_{BZ}$ seem to be smaller compared to those that correspond to $MWCNT_{ACN}$ (inset Fig. 8). Anyhow, a quantitative estimation of the R_{ct} values and the other EIS parameters corresponding to the investigated systems can be determined by fitting the experimental impedance spectra with the appropriate equivalent electrical circuit. As a first approximation, the impedance responses of the investigated electrodes were modeled with the Randles electrical circuit [41, 42]. The Randles circuit ($R_s + (C_{dl}/R_{ct} + Z_w)$) (Fig. 9), which is used very often to describe electron transfer reactions at a planar electrode/film surface, has a clear physical meaning. This circuit includes a resistance in series with a parallel combination of a capacitive path and charge transfer path [43]. The

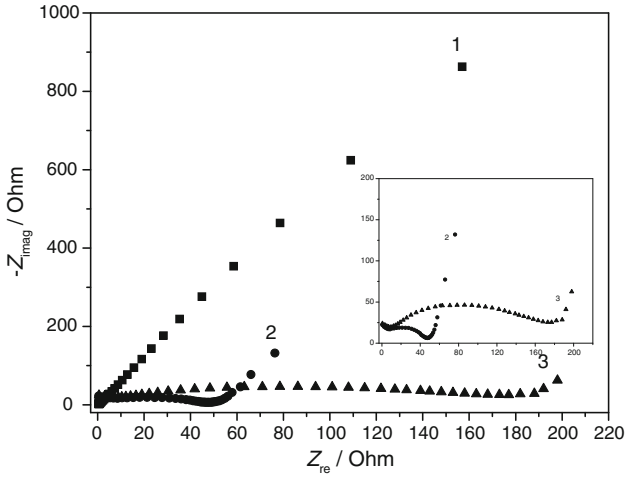

Fig. 8 EIS spectra recorded for $CoCp_2$ (1.0×10^{-3} mol dm^{-3}) in ACN (0.1 mol dm^{-3} $TBAPF_6$) on GC (*1*), $MWCNT_{BZ}$ (*2*), and $MWCNT_{ACN}$ (*3*) electrodes in the frequency range from 1 to 50 kHz. For better readability the solution ohmic resistance R_s was subtracted from the real part of the impedance data. *Inset* zoom of the impedance behavior of the $MWCNT_{BZ}$ (*2*) and $MWCNT_{ACN}$ (*3*) films

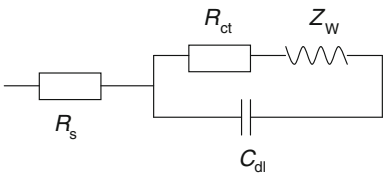

Fig. 9 The equivalent circuit used for fitting the EIS data obtained for the investigated systems MWCNT/$CoCp_2$/electrolyte and GC/$CoCp_2$/electrolyte. R_s, electrolyte resistance; C_{dl}, double layer capacitance; R_{ct}, charge transfer resistance; Z_W, Warburg impedance (software Thales, version 4.15). In this model the upper branch (R_{ct} and Z_W) represents the electron transfer and diffusion processes involving the redox couple (Faradaic redox reaction), which occur in parallel with the charging of the capacitor (the lower branch, C_{dl})

series resistance (R_s) represents the resistance of the electrolyte fluid plus the resistance of cables and wires connecting the electrode to the instrument; the double layer capacitance (C_{dl}) is made up of charges in the working electrode and ions in the solution; the charge transfer resistance (R_{ct}) is kinetically controlled and represents current flow via redox reactions at the electrode–fluid interface (electron transfer resistance between the redox couple and the electrode); and Z_W is the well-known Warburg impedance element, is mass transfer controlled, and arises physically from mass transport limits of ions in the solution (diffusion impedance of the redox couple in solution). Because the ionic diffusion and the heterogeneous charge transfer occur as successive mechanisms, the Warburg impedance Z_W is connected in series with the resistance R_{ct}, which in turn are connected in parallel with C_{dl}. The chosen equivalent electrical circuit was found to give adequate fits of the impedance data. The obtained maximum % mean error from the simulation was found to be around 0.9% in all cases and was considered to be acceptable. The determined EIS parameters for the investigated electrodes are included in Table 1. As was mentioned above the Warburg impedance is created by the diffusion of charge carriers and depends strongly on the frequency range used for the EIS experiments. At high frequencies the Warburg impedance appears to be relatively small, because diffusion reactants are not moved very far, whereas when the frequency decreases the reactants have to diffuse even farther and therefore the Warburg impedance increases. The Warburg impedance is given by the following relation [44]:

$$Z_W = \frac{\sigma}{\sqrt{i\omega}} \tag{3}$$

where ω is the angular frequency and σ is the Warburg parameter that includes the diffusion coefficient. The σ coefficient, which is strongly dependent on the diffusion ability of the species, is given by the following relation:

$$\sigma = \frac{RT}{n^2F^2A\sqrt{2}}\left(\frac{1}{C_o\sqrt{D_o}} + \frac{1}{C_R\sqrt{D_R}}\right) \tag{4}$$

where D_o and D_R are the diffusion coefficients of the oxidized and reduced species, respectively; and C is the bulk concentration of the diffused species. The determined values of the mass transfer impedance component σ are included in Table 1. As can be seen, the σ values decrease in the following order: GC (34.06 kΩ $s^{-1/2}$) > $MWCNT_{BZ}$ (0.32 kΩ $s^{-1/2}$) > $MWCNT_{ACN}$ (0.25 kΩ $s^{-1/2}$), indicating that the diffusion ability of the reactants is enhanced on MWCNT films, whereas on the GC electrode their ability for diffusion is rather small. However, among the MWCNT investigated the one formed upon decay of BZ seems to have a slightly larger σ coefficient. Furthermore, the EIS results indicate that the charge transfer resistance obtained on the $MWCNT_{BZ}$ film (R_{ct} = 42.9 Ω) is relatively small, whereas obviously the charge transfer resistance of the $MWCNT_{ACN}$ film (R_{ct} = 170.0 Ω) seems to be much larger. The smaller R_{ct} value obtained for $MWCNT_{BZ}$ can be mainly attributed to the increase of the effective surface area of the film which leads to an enhancement of its quality and thus its sensitivity [45]. Furthermore, the fact that the $MWCNT_{BZ}$ film is more conductive than $MWCNT_{ACN}$ additionally improves its quality as an electrode. The GC electrode, as expected, is characterized by the smallest charge transfer resistance (R_{ct} = 22.8 Ω), therefore verifying the reversible behavior of the $CoCp_2^{+/0}$ couple, which was observed for this electrode. The R_{ct} is related to the reaction kinetics by the Butler–Volmer equation for a charge-transfer-controlled electrochemical reaction [46, 47]:

$$R_{ct} = \frac{RT}{nFI_o} \tag{5}$$

where I_o represents the exchange current of the reaction. The I_o values for the investigated electrodes were calculated from the simulated R_{ct} values using Eq. 5 and are included in Table 1. Considering that the relationship between the exchange current I_o and the standard rate constant k_s is given by the equation $I_o = nFAk_sC$ [48] (where A is the electrode active surface area and C is the concentration of the electro-active species), Eq. 5 is converted to the following relation, which indicates that R_{ct} varies inversely with k_s:

$$R_{ct} = \frac{RT}{n^2F^2Ak_sC} \tag{6}$$

It is interesting that in the present work the R_{ct} parameters of the investigated films varied inversely with the kinetic parameter k_s determined on these electrodes, therefore indicating that k_s significantly affects the impedance behavior of the electrodes. It is, thus, noticeable that in the case of $MWCNT_{ACN}$, having the smallest k_s value ($k_s \approx 1 \times 10^{-3}$ cm s^{-1}), the impedance semicircle dominates in the high frequency region of the EIS spectrum, because the slow charge transfer kinetics largely controls the electrochemical response on the film. Equation 6 is very useful because it offers the possibility of calculating the k_s when R_{ct} is obtained by fitting the experimental EIS data. A comparison of the k_s values obtained from CV and EIS data is shown in Table 1. As can be seen the agreement is very good.

The C_{dl} values increase in the following order: $MWCNT_{ACN}$ (1.20 μF) < $MWCNT_{BZ}$ (2.42 μF) < GC (11.62 μF). The extracted results suggest that from all investigated electrodes the GC has the greater double layer capacitance. However, of the investigated MWCNT films

the one produced upon decomposition of BZ seems to have the greater C_{dl} most probably because of its high degree of roughness which characterizes this film. It is well known that C_{dl} depends on many variables such as electrode potential, temperature, ionic concentrations, type of ions, oxide layers, electrode roughness, and impurity adsorption.

Conclusions

In the present work MWCNT films were produced by catalytic CVD on SiO_2 substrate upon decomposition of either BZ or ACN using $FeCp_2$ as catalyst. The sensitivity of the synthesized MWCNT films to the oxidation of $CoCp_2$ to $CoCp_2^+$ in ACN was tested by CV and EIS. In general, the extracted results reveal that both MWCNT films exhibit sensitivity to $CoCp_2$. It is, however, obvious that $MWCNT_{BZ}$ produced upon decay of BZ seem to be a better choice for electrode materials rather than $MWCNT_{ACN}$ because they are better capacitors and provide less Warburg impedance and less charge transfer resistance, therefore supporting fast electron transfer kinetics. The reason for this behavior seems to be the increased roughness which characterized the $MWCNT_{BZ}$ films. The findings of the present work reveal that $MWCNT_{BZ}$ films are promising electrode materials for electrochemical identification, quantification, and characterization of electro-active species in organic solvent media.

Experimental

Chemicals and solutions

Acetonitrile (Merck, puriss. grade) was distilled over phosphorus pentoxide and then redistilled over potassium carbonate. Cobaltocene ($CoCp_2$, Merck, puriss. grade) was purified by vacuum sublimation. Tetrabutylammonium hexafluorophosphate ($TBAPF_6$, Fluka, purum grade) was recrystallized twice from absolute ethanol and dried under reduced pressure at the room temperature for 12 h. The solids were stored under argon in Schlenk tubes. For the measurements a concentrated solution of $TBAPF_6$ (0.1 mol dm^{-3}) in ACN was used for the preparation of the dilute solution of $CoCp_2$ (1.0×10^{-3} mol dm^{-3}). The solutions were prepared under argon using Schlenk techniques. It is well known that the presence of impurities such as water and oxygen can significantly influence the kinetic results in non-aqueous solvents. Furthermore, $CoCp_2$ can be readily oxidized by air and water and therefore the use of argon during the measurements was considered to be essential.

Synthesis of MWCNT films

Vertically aligned $MWCNT_{BZ}$ and $MWCNT_{ACN}$ were selectively synthesized on SiO_2 substrate film (geometrical area 0.5 cm^2) in a furnace by catalytic CVD using $FeCp_2$ as catalyst precursor and either BZ or ACN as carbon source, respectively. The $FeCp_2$ solution (1% w/w) in either BZ or ACN was introduced into the furnace through a syringe at a flow rate of 0.2 cm^3 min^{-1} at a temperature of 900 °C. The synthesis process was performed using argon as carrier gas. The CVD set-up and the catalysis method which was followed were reported previously [49–51]. The resultant $MWCNT_{BZ}$ and $MWCNT_{ACN}$ films were characterized extensively using SEM, TEM, TGA, and Raman spectroscopy.

Apparatus

The cyclic voltammograms were recorded using a computer-controlled Zahner/IM6/6EX system. The effect of the uncompensated resistance was reduced by using the positive feedback technique. However, to avoid overcompensation and consequently circuit oscillation, only 85% of the uncompensated resistance was compensated. The measurements were carried out using a three-electrode cell configuration. The working electrodes used were $MWCNT_{BZ}$ (active surface area 0.64 cm^2), $MWCNT_{ACN}$ (active surface area 0.31 cm^2), and GC (active surface area 0.08 cm^2). The counter electrode was a Pt plate, whereas the reference electrode was Ag/AgCl (KCl sat.). The measuring cell used was a three-compartment cell designed to minimize the distances between the electrodes with a total solution volume of ca. 20 cm^3. Before each measurement process the solution was purged with high purity argon to eliminate interference from oxygen. The cyclic voltammograms were recorded in the potential region from −1.5 to 0 V vs. Ag/AgCl (KCl sat.) with scan rates (v) ranging from 0.04 to 0.15 V s^{-1}. All measurements were carried out at 294.15 ± 0.5 K.

The EIS spectra were recorded using the computer-controlled Zahner/IM6/6EX system by applying a small ac amplitude (10 mV) in a wide frequency range (from 1 to 50 kHz) at 294.15 ± 0.5 K. All measurements were performed on either $MWCNT_{BZ}$, $MWCNT_{ACN}$, or GC working electrodes against the reference electrode Ag/AgCl (KCl sat.), whereas a Pt plate served as counter electrode. The EIS spectra were recorded at the formal potential of the $CoCp_2^{+/0}$ redox couple (in the potential region from −0.93 to −0.90 V vs. Ag/AgCl). The EIS spectra were analyzed using the electrochemistry software package Thales (version 4.15).

SEM pictures of the produced $MWCNT_{BZ}$ and $MWCNT_{ACN}$ films were obtained on an FEI/Philips (model

XL30 ESEM) computer-controlled scanning electron microscope with an accelerating voltage of 10 kV and magnification factor of either ×2,000 or ×2,560. The Raman scattering measurements of the synthesized MWCNT were carried out using a Jasco RFT-6000 FT-Raman attachment coupled with an FT/IR-6300 spectrometer at an excitation wavelength of 1,064 nm (excitation energy of 1.17 eV). The Raman spectra were recorded by using laser power of 50–200 mW and spectral resolution of 4 cm^{-1} in the backscattering geometry.

Acknowledgments The authors would like to thank D. Schneider, S. Heusing, and C. Siegmund (TU Ilmenau).

References

1. Radushkevich LV, Lukyanovich VM (1952) Zurn Fisic Chim 26:88
2. Wiles PG, Abrahamson J (1978) Carbon 16:341
3. Iijima S (1991) Nature 354:56
4. Merkoci A (2006) Microchim Acta 152:157
5. Tasis D, Tagmatarchis N, Bianco A, Prato M (2006) Chem Rev 106:1105
6. Zheng LX, O'Connell MJ, Doorn SK, Liao XZ, Zhao YH, Akhadov EA, Hoffbauer MA, Roop BJ, Jia QX, Dye RC, Peterson DE, Huan SM, Liu J, Zhu YT (2004) Nat Mater 3:673
7. Inoue T, Gunjishima I, Okamoto A (2007) Carbon 45:2164
8. Banks CE, Compton RG (2006) Analyst 131:15
9. Gommes C, Blacher S, Bossuot C, Marchot P, Nagy JB, Pirard JP (2004) Carbon 42:1473
10. Cantoro M, Hofmann S, Pisana S, Scardaci V, Parvez A, Ducati C, Ferrari AC, Blackburn AM, Wang KY, Robertson J (2006) Nano Lett 6:1107
11. Bladh K, Falk LKL, Rohmund F (2000) Appl Phys A Mater Sci Process 70:317
12. Gooding JJ (2005) Electrochim Acta 50:3049
13. Wang J (2005) Electroanalysis 17:7
14. Campbell JK, Sun L, Crooks RM (1999) J Am Chem Soc 121:3779
15. Deo RP, Wang J (2004) Electrochem Commun 6:284
16. Musameh M, Wang J, Merkoci A, Lin Y (2002) Electrochem Commun 4:743
17. Ye JS, Wen Y, Zhang WD, Gan LM, Xu GQ, Sheu FS (2003) Electroanalysis 15:1693
18. Wang J, Li M, Shi Z, Li N, Gu Z (2002) Anal Chem 74:1993
19. Salimi A, Hallaj R, Khayatian GR (2005) Electroanalysis 17:873
20. Punbusayakul N, Talapatra S, Ci L, Surareungchai W, Ajayan PM (2007) Electrochem Solid-State Lett 10:13
21. Tsierkezos NG (2008) J Mol Liq 138:1
22. Dresselhaus MS, Dresselhaus G, Saito R, Joiro A (2005) Phys Rep 409:47
23. Popov VN, Henrard L, Lambin P (2009) Carbon 47:2448
24. Ferrari AC, Robertson J (2000) Phys Rev B Condens Matter Mater Phys 61:14095
25. Bard AJ, Garcia E, Kukharenko S, Strelets VV (1993) Inorg Chem 32:3528
26. Connelly NG, Geiger WE (1996) Chem Rev 96:877
27. Geiger WE (1974) J Am Chem Soc 96:2632
28. Stojanovic RS, Bond AM (1993) Anal Chem 65:56
29. Koelle U (1978) J Organomet Chem 152:225
30. Santucci R, Faraoni A, Campanella L, Tranchida G, Brunori M (1991) Biochem J 273:783
31. Nicholson RS (1965) Anal Chem 37:1351
32. Yu J, Flavel BS, Shapter JG (2008) Fuller Nanotub Carbon Nanostruct 16:18
33. Noel M, Suryanarayanan V, Santhanam R (2000) Electroanalysis 12:1039
34. Rodriguez Nieto JF, Tucceri RI, Posadas D (1996) J Electroanal Chem 403:241
35. Macdonald JR (1987) Impedance spectroscopy: emphasizing solid materials and systems. Wiley, New York
36. Mohran HS (2005) Am J Appl Sci 2:1629
37. Djellal L, Bouguelia A, Trari M (2008) Semicond Sci Technol 23:45019
38. Bardea A, Patolsky F, Dagan A, Willner I (1999) Chem Commun 21
39. Esplandiu MJ, Pacios M, Bellido E, Del Valle M (2007) Z Phys Chem 221:1161
40. Barbero C, Tucceri RI, Posadas D, Silber JJ, Sereno L (1995) Electrochim Acta 40:1037
41. Randles JEB (1948) Trans Faraday Soc 44:327
42. Vetter KJ (1967) Electrochemical kinetics. Academic, New York
43. Omeiri S, Bellal B, Bouguelia A, Bessekhouad Y, Trari M (2009) J Solid State Electrochem 13:1395
44. Koeleli F, Roepke T, Hamann CH (2003) Electrochim Acta 48:1596
45. Yu J, Li J, Zhao F, Zeng B (2008) J Braz Chem Soc 19:849
46. Bard AJ, Faulkner LR (1980) Electrochemical methods. Wiley, New York
47. Sundfors F, Bobacka J, Ivaska A, Lewenstam A (2002) Electrochim Acta 47:2245
48. Suresh P, Shukla AK, Munichandraiah N (2002) J Appl Electrochem 32:267
49. Rao CNR, Sen R, Satishkumar BC, Govindaraj A (1998) Chem Commun 1525
50. Satishkumar BC, Govindaraj A, Rao CNR (1999) Chem Phys Lett307:158
51. Weber L, Kloeckner K, Ritter U, Scharff P (2009) Russ J Electrochem 45:1145
52. Aoki K, Kaneko H, Nozaki K (1988) J Electroanal Chem 247:29